ORIGINAL PAPER

Electrical conductivity and dielectric relaxation studies on microwave synthesized $Na_2SO_4 \cdot NaPO_3 \cdot MoO_3$ glasses

B. Sujatha[1] · R. Viswanatha[2] · B. K. Chethana[2] · H. Nagabhushana[3] ·
C. Narayana Reddy[4]

Abstract Electrical conductivity and dielectric relaxation studies on SO_4^{2-} doped modified molybdo-phosphate glasses have been carried out over a wide range of composition, temperature and frequency. The d.c. conductivities which have been measured by both digital electrometer (four-probe method) and impedance analyser are comparable. The relaxation phenomenon has been rationalized using electrical modulus formalism. The use of modulus representation in dielectric relaxation studies has inherent advantages viz., experimental errors arising from the contributions of electrode-electrolyte interface capacitances are minimized. The relaxation observed in the present study is non-Debye type. The activation energies for relaxation were determined using imaginary parts of electrical modulus peaks which were close to those of the d.c. conductivity implying the involvement of similar energy barriers in both the processes. The enhanced conductivity in these glasses can be attributed to the migration of Na^+, in expanded structures due to the introduction of SO_4^{2-} ions.

✉ C. Narayana Reddy
  nivetejareddy@gmail.com

1 Department of Electronics and Communication, MSR Institute of Technology, Bangalore 560054, India

2 Solid State and Structural Chemistry Unit, Indian Institute of Science, Bangalore 560012, India

3 Department of Physics, Tumkur University, Tumkur 572103, India

4 Department of Physics, Sree Siddaganga College of Arts, Science and Commerce, B H Road, Tumkur 572102, India

Introduction

The need for electrolytes suitable for battery applications has spurred investigations into a number of silver/alkali ion conducting glasses [1–9]. The quest for such inorganic vitreous electrolytes with exceptional thermal and electrical properties has opened up a new generation of superionic glasses. It is apparent that two strategies have been used to design fast ion conducting (FIC) electrolytes. The first is to combine two anionic species, which has been known to give enhanced conductivity and is called the mixed anionic effect [1]. The second strategy is to dissolve highly ionic salts such as $Li_2SO_4/Na_2SO_4/Ag_2SO_4$ and alkali halides [10–15]. Conductivity enhancement can also be achieved by the addition of more than one glass former to the modifier oxide. Incorporation of large anions such as SO_4^{2-}, S^{2-}, SO_3^{2-}, Cl^-, and Br^- etc. results in "loosening" of the interstitial glass structure. As a consequence, activation energy decreases, whereas the conductivity itself increases [10, 11].

The use of microwaves for the synthesis of inorganic compounds has gained great importance in the recent years [16]. They include sintering of ceramics [17, 18], microwave-assisted precipitations [19], sol-gel [20] and hydrothermal [21] processes. Relatively fewer reports have appeared on microwave-assisted solid synthesis [22]. This method is extensively used to prepare nanomaterials [23–26]. To our knowledge, there have been no reports of microwave-assisted solid state synthesis of alkali salt doped glasses in literature. Microwave method offers several advantages over conventional melt quench technique, the most important of them being reduced reaction time and energy efficiency. This fast process reduces volatilization of ingredients and also limits the diffusion of elements from crucible to the melt. One of the important requirements of this method is that at least one of the reactants should be a microwave susceptor. In

this paper, we report conductivity and dielectric relaxation of glasses prepared by simple microwave method, which contains up to 25 mol% of Na_2SO_4 and less than 20 mol% of MoO_3 content in a phosphate host matrix. Also, an attempt has been made to obtain activation energies using ab initio density functional calculations.

Experimental

Glasses in the system $xNa_2SO_4 \cdot (100-x)[0.8NaPO_3:0.2MoO_3]$ (where $5 \leq \times \leq 25$) were prepared by employing a simple energy-efficient microwave heating method. Reagent (AR) grade sodium sulphate (Na_2SO_4), sodium dihydrogen orthophosphate ($NaH_2PO_4 \cdot 2H_2O$) and molybdenum trioxide (MoO_3) were used as starting materials. In the synthesized glass system, both MoO_3 and $NaH_2PO_4 \cdot 2H_2O$ are microwave susceptors [27]. Appropriate amounts of starting materials were thoroughly ground to homogenize the mixture and kept in a clean silica crucible on a fire brick inside a domestic microwave oven (LG-1291 HE model) operating at 2.4 GHz and a tuneable power level up to a maximum of 850 W; microwaves were switched on, and within 2 to 3 min of exposure, complete decomposition of $NaH_2PO_4 \cdot 2H_2O$ to $NaPO_3$ and water vapour was achieved. A good homogenous melt, which was obtained after 6 to 7 min (which is only a fraction of time required in conventional glass preparation methods), was quenched between preheated (60 °C) brass plates. The silica crucible was found to remain clean and unaffected during the short duration of melting. The glass was annealed in a muffle furnace for 2 h at 200 °C to remove thermal strains that could have developed during quenching. The samples were preserved in a sealed desiccator containing $CaCl_2$.

The density of the samples was measured by the Archimedes' liquid displacement method $\rho = \frac{W_1}{W_1-W_2}\rho_L$ where W_1 and W_2 are the weights of the sample in air and liquid, respectively, ρ_L is the density of the immersion liquid. Molar volume M_v was calculated using $M_v = \frac{M}{\rho}$, where M is the molecular weight of the sample. The relative error in the measurement of density was about ±0.005 g cm^{-3}. Vickers hardness was measured using TTS unlimited, Inc. Japan, HWMMT-model, with a Vickers indenter. The surface of the glass sample was cleaned using 10 % HF aqueous solution, and the applied load and loading time were 0.245 N and 30 s, respectively. The indentation of the glass sample was observed using a microscope at room temperature.

The samples were crushed in a mortar to a fine powder and tested for the amorphous nature of glass using a powder diffractometer (model: Rigaku DMAX-IC employing Cu-K$_\alpha$ radiation). Glass transition temperature (T_g) of the samples were recorded using a differential scanning calorimeter (Perkin

Elmer DSC-2): random pieces of glass samples (15 mg) were placed in a platinum crucible and heated up to 900 K in an argon medium at a heating rate of 2 K/min. Alumina powder was used as reference material and the accuracy in the measurement of T_g was ±2 K.

The annealed samples were thoroughly polished and coated with silver paste on both sides, which serve as electrodes having a thickness of about 0.1 cm and a diameter of about 0.8 cm for electrical measurements. Resistance of the samples were calculated by measuring the applied voltage (2 V) and current through the sample (using a digital electrometer ECIL EA-5600). The temperature was measured using a chromel-alumel thermocouple placed very close to the sample. Impedance measurements were also carried out for all the investigated glasses using Hewlett-Packard HP 4192A impedance-gain phase analyser from 10 Hz to 10 MHz in the temperature range 300–380 K. A home-built cell assembly (having two terminal capacitor configurations and spring-loaded silver electrodes) was used for the measurements. The temperature was controlled using PID temperature controller (Heatcon, Bangalore 560090, India) with an accuracy of ±1K, in the entire range of measurements. The temperature of the sample was measured using Pt-Rh thermocouple positioned very close to the electrode.

The glass structures were optimized by density functional theory (DFT) employing B3LYP functional using Gaussian 09 suite [28]. The LANL2DZ [29] effective core potentials were used for the molybdenum, and 6-311++g (d) [30] basis set was used for the H, O, Si and Na atoms. Energy was calculated for the stationary points and characterized as true minima. Transition state structures were analysed by the presence of an imaginary frequency and confirmed by intrinsic reaction coordinate (IRC) calculations and the energies are listed in Table 1.

Results and discussion

Codes of the samples, composition, molar volume, Vickers hardness, glass transition temperature, activation energies (E_{dc} and E_{ac}) and glass transition width are listed in Table 1. XRD patterns exhibit only a broad hump-like feature in the low-angle region, characteristic of an amorphous nature. Further, the observation of characteristic glass transition temperature extracted from DSC thermograms also confirms the glassy nature of the sample.

Physical and thermal properties

A typical modulated DSC thermogram shown in Fig. 1 is used to extract glass transition temperature (T_g) and glass transition width $(\Delta T_g) = T_1 - T_g$, where T_1 is the liquidus temperature. As

Table 1 Code, composition, ρ, M_v, T_g, H_v, ΔT_g, E_{dc} and E_{ac} of the investigated glasses

Code	Composition (mol%)				$\rho \pm 0.005$ g cm^{-3}	$M_v \pm 0.5$ cm^3	$T_g \pm 1$ K	H_v (kgmm^{-2})	$E_{dc} \pm 0.002$ eV	$E_{ac} \pm 0.002$ eV	ΔT_g,K	$E_{ac} \pm 0.002$ (DFT)(eV)
	Na$_2$SO$_4$	Na$_2$O	P$_2$O$_5$	MoO$_3$								
NPM1	05	38	38	19	3.215	35.211	541	412	0.666	0.642	13.1	0.73
NPM2	10	36	36	18	3.125	36.292	533	404	0.630	0.621	13.0	0.71
NPM3	15	34	34	17	3.039	36.639	520	386	0.620	0.601	12.93	0.68
NPM4	20	32	32	16	2.939	41.115	512	384	0.591	0.553	12.89	0.65
NPM5	25	30	30	15	2.854	41.654	505	362	0.534	0.531	12.80	0.61

can be seen from Table 1, both T_g and H_v (Vickers hardness) decrease with increasing Na$_2$SO$_4$ mol% [31]. The structure-sensitive parameter, T_g mainly depends on the bond strength, cross-link density and effective packing of structural species [32]. It has been suggested that addition of Na$_2$SO$_4$ makes the glass structure less rigid by expanding the network isotropically. A similar observation was made by Button et al. [33] in LiCl-containing glasses. They have reported that the network is systematically weakened and expanded as the halide is accommodated in the glass matrix.

Physical and thermal properties of the investigated glasses are strongly dependent on composition. In NaPO$_3$ glass, $\frac{Na_2O}{P_2O_5}$ $= 1$ and consists of long phosphate chains. The metaphosphate chains can also give rise to closed rings. The presence of such chains and rings has been reported in chromatograph studies [34], hence, truncated chains, in which phosphate tetrahedra possess three unshared oxygen corners [1]. The modification of such network implies breaking of bonds by the added oxygen ions while MoO$_3$ remains in the structure as [MoOO$_{5/2}$]$^-$. These units are attached to [POO$_{2/2}$O]$^-$ units (discussed in "d.c. conductivity and activation energy") since

the electronegativity of [POO$_{3/2}$]^0 is greater than [MoOO$_{5/2}$]$^-$. The added Na$_2$SO$_4$ salt is dissolved (Na$_2$SO$_4 \rightarrow$ 2Na$^+$ +SO$_4^{2-}$) in the molybdo-phosphate glass matrix. However, SO$_4^{2-}$ ions and metaphosphate units appear to interact weakly, resulting in a dynamic concentration of dithiophosphate [DTP] units. This dynamical character of DTP was suggested as capable of assisting alkali ion transport as well [34].

The variation of glass transition temperature as a function of Na$_2$SO$_4$ concentration is consistent with the free volume model of glass transition [35]. The free volume available in the molten phase is more effectively utilized for transport by discrete anions along with the cations. The excess free volume frozen in glass would be due to the isotropic dissolution of Na$_2$SO$_4$, which causes a volume increasing effect. Consequently, density, Vickers hardness, structural rigidity and T_g decrease with increasing concentration of sodium salt. Examination of the specific heat capacity versus temperature reveals that the width of the glass transition, ΔT, was found to be 13.1–12.8 K, suggesting that the investigated glasses were fragile. Moynihan et al. reported that glasses displaying widths $\Delta T > 30$ K are strong [36].

d.c. conductivity and activation energy

The d.c. conductivities of the same glass composition but prepared in different batches showed agreement within 5 % error. Figure 2 shows the variation of log (σ) as a function of inverse temperature for different MoO$_3$ concentrations. It can be inferred from Fig. 2, conductivity values of NPM5 glass lie in the range 7.447×10^{-6} to 5.584×10^{-4} S/cm when the temperature varied from 300 to 380 K. Also, it is seen from Fig. 2 that all the investigated samples follow Arrhenius law, and the solid line represents the linear least square fits of linear regression used to obtain the activation energy (E_{dc}). The values of E_{dc} lie in the range of 0.534–0.666 eV and are listed in Table 1.

Cole–Cole plots at five different temperatures for the NPM1 glass are presented in Fig. 3. The plots for all the investigated glass samples were found to be good semicircles with a spur. The semicircles of the impedance plot, $-Z''$ versus
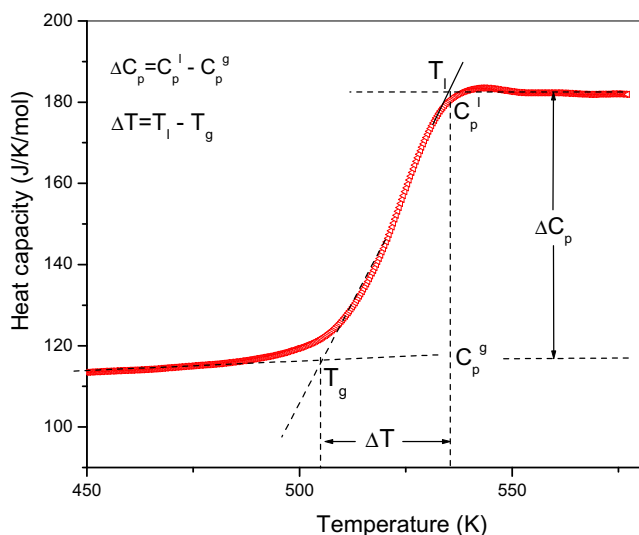

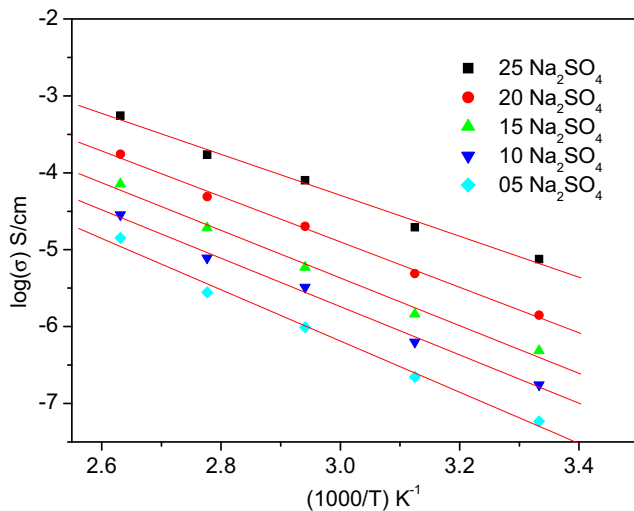
Fig. 1 Modulated DSC thermogram of NPM5 glass

Fig. 2 Variation of log (σ) versus (1000/T)

Z', were used to determine the bulk resistance. The intersection point of the low frequency end of the high frequency arc gives resistance and was used for calculating d.c. conductivities. A characteristic spur at low frequencies points to blocking of Na^+ ions at the silver electrodes. Besides, the centre of the semicircle is depressed below the real axis, suggesting an associated relaxation of ions that is non-Debye type [37]. Arrhenius plot of $log(\sigma)$ versus (1000/T), and the regression data is shown in Fig. 3 (inset). The activation energy obtained from this plot using linear regression is 0.65 eV, which is in close agreement with E_{dc} values listed in Table 1. Also, σ_{dc}, an increase with increase in concentration of Na_2SO_4, is two orders of magnitude for an increase of Na_2SO_4 from 5 to 25 mol%.

Real and imaginary parts of complex impedance contain information on the kinetics of electrical relaxation in bulk glassy material. The asymmetric variation in the broadening
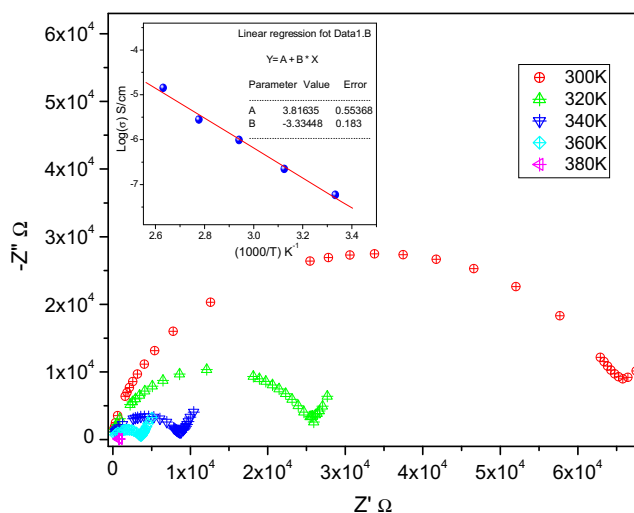
of Z'' suggests that there is a spread in relaxation time, i.e. the existence of a temperature-dependant electrical relaxation phenomenon in the material [38]. A number of literature reports are available on models developed for explaining the conduction process in solid electrolytes [39–43]. These reports emphasize the role of various factors such as composition, structure, conductivity and diffusion process in the development of the models. However, the model proposed by Dyre et al. [39, 43] is found to be commonly employed to describe ion conduction mechanism. Besides this, the other commonly used models include molecular dynamic simulation approach based on diffusion [41], dynamic structure model [42] and weak electrolyte theory [44]. The weak electrolyte theory was developed by Ravaine et al. [44] based on the thermodynamic approach developed for liquid electrolyte systems with different dopants, such as alkali halides and alkali oxysalts [45, 46]. According to the above model, the conductivity enhancement depends on concentrations of mobile ions.

Figure 4 and its inset illustrate the real and imaginary parts of impedance (Z' and Z'') with frequency at different temperatures. As can be seen from Fig. 4, Z' gives a dip prior to merger at high frequency and decreases with increasing temperature. However, Z'' values increase with frequency and reach a maximum, and the peak (Z''_{max}) shifts to higher frequencies with increasing temperature. The asymmetric nature of Z'' with frequency suggests a spread in relaxation process of conduction [9]. The effect on relaxation time, τ_0, is discussed later.

In order to examine the variations observed in both conductivity and activation energy of alkali (Na_2O) modified molybdo-phosphate glasses, it is necessary to consider the effect of network modification, which reveals the nature and concentration of structural units. Besides network modification, isotropic dissolution of Na_2SO_4 plays a crucial role because
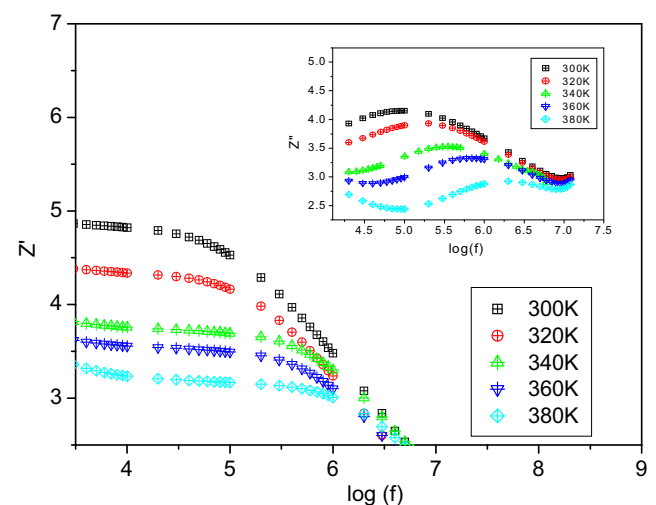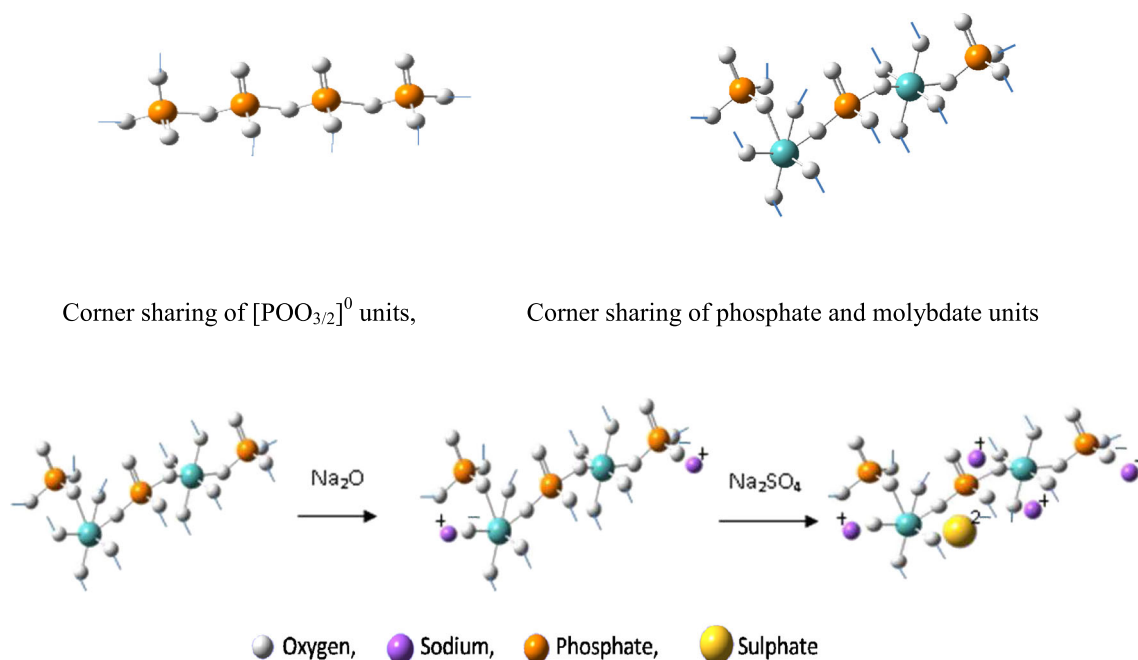

Fig. 3 Cole-Cole plot of NPM 1 glass. Inset: Arrhenius plot of NPM 1 glass with linear regression data

Fig. 4 Variation of Z' versus log (f) for NPM3 glass. *Inset*: variation of Z'' versus log (f)

SO_4^{2-} ions occupy the interstitial positions. The basic structure of molybdo-phosphate glass containing octahedral $[MoO_{6/2}]^0$ units and tetrahedral $[POO_{3/2}]^0$ units by corner sharing through oxygen is shown in Scheme 1.

Hence, the basic structure of molybdo-phosphate glass consists of *Mo*-O-Mo, Mo-O-P and P-O-P linkages. Every $[POO_{3/2}]^0$ tetrahedron provides three corners for the oxygen sharing and a molecule of P_2O_5 creates three such tetrahedra, and the connectivities are in accordance with the proportion of glass-forming oxides. The network modification requires the oxide ion (O^{2-}) of the modifier to reach the site where bond breaking takes place. Since the oxide ion carries a negative charge of two units, they drift towards a linkage where the columbic interaction is energetically favourable. The bond energies are such that $E_{Mo\text{-}O\text{-}Mo} < E_{Mo\text{-}O\text{-}P} < E_{P\text{-}O\text{-}P}$ [47]. The effect of modifier oxide is to break various linkages, and the order of easiness of bond breaking is Mo-O-Mo > Mo-O-P > P-O-P sequentially. The bond breaking results in the formation of non-bridging oxygens when Na_2O is added to the molybdo-phosphate network. The modification can be represented as $30Na_2O + 30P_2O_5 + 15MoO_3 \equiv 60\ Na^+ + 30O^{2-} + 60[POO_{3/2}]^0 + 15[MoO_{6/2}]^0 \rightarrow 60\ Na^+ + 15[MoOO_{5/2}]^- + 45\ [POO_{2/2}O]^- + 15[POO_{3/2}]^0$. The resultant structural units are listed in Table 2. The modifier role of Na_2O is the most dominant factor, follows the well-known successive degradation of the network [48] and results in the formation of anionic species. The alkali salt (Na_2SO_4) dissolves in a polymeric sodium-molybdo-phosphate network, as SO_4^{2-} ions occupy interstitial positions. There have been suggestions of SO_4^{2-} ions being

incorporated into the network [49]. Currents passed in conductivity experiments are usually in nanoamperes and cause very insignificant electrolysis. We intend to emphasize the fact that introduction of SO_4^{2-} ions increases the effective mobility of Na^+ ions leading to greater conductivity. The concentrations of Na^+ and SO_4^{2-} ions are calculated by the method given by Sathyanarayana et al. [50] and are listed in Table 2. It is evident from above that as the concentration of Na_2SO_4 increases, the population of both Na^+ and SO_4^{2-} ions in the network increases; further, the concentration of $[SO_4^{2-}]$ increases the network volume. Consequently, conductivity increases while activation energy decreases. Further, Na^+ ions are present in the columbic wells surrounded by sulphatic oxygens, are expected to be shallow and therefore are characterized by a lower activation barrier for Na^+ ion transport. Such Na^+ ions are likely to dominate the conduction process [1]. Glasses containing transition metal ions (TMI) are present in more than one valence state, and hopping of electrons via aliovalent states is responsible for conduction. The addition of Na_2O to molybdophosphate network breaks the Mo^{5+}–O–Mo^{6+} linkages along with Mo–O–P, P–O–P and forms the structural defects. When the MoO_3 content is less than 30 mol% in the glass system, ionic conductivity dominates [51].

Ab initio calculations were performed to gain further molecular-level understanding of the activation energy for ion transport in molybdophosphate glasses and compared with the experimental activation energies. Based on experimental and theoretical studies, it has been suggested that the hopping/transfer of Na^+ to the neighbouring oxygen leads to the
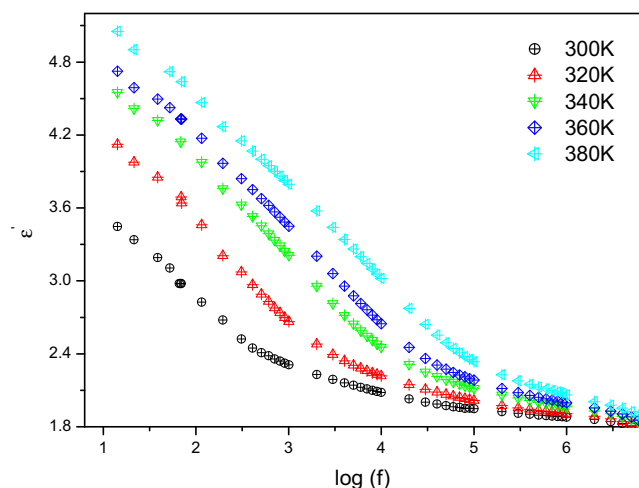

Corner sharing of $[POO_{3/2}]^0$ units,   Corner sharing of phosphate and molybdate units

Oxygen,   Sodium,   Phosphate,   Sulphate

Scheme 1 The structural model used for the ab initio calculations

**Table 2**   Code, network modification and concentration of [Na$^+$] and [SO$_4^{2-}$] ions

Code	Network modification	[Na$^+$] ions/mol	[SO$_4^{2-}$] ions/mol
NPM1	19[MoOO$_{5/2}$]$^-$, 57[POO$_{2/2}$O]$^-$, 19[POO$_{3/2}$]^0, 86Na$^+$, 5SO$_4^{2-}$	1.471 × 10^{22}	0.34 × 10^{22}
NPM2	18[MoOO$_{5/2}$]$^-$, 54[POO$_{2/2}$O]$^-$, 18[POO$_{3/2}$]^0, 92Na$^+$, 10SO$_4^{2-}$	1.54 × 10^{22}	0.67 × 10^{22}
NPM3	17[MoOO$_{5/2}$]$^-$, 51[POO$_{2/2}$O]$^-$, 17[POO$_{3/2}$]^0, 98Na$^+$, 15SO$_4^{2-}$	1.59 × 10^{22}	0.979 × 10^{22}
NPM4	16[MoOO$_{5/2}$]$^-$, 48[POO$_{2/2}$O]$^-$, 16[POO$_{3/2}$]^0, 104Na$^+$, 20SO$_4^{2-}$	1.62 × 10^{22}	1.167 × 10^{22}
NPM5	15[MoOO$_{5/2}$]$^-$, 45[POO$_{2/2}$O]$^-$, 15[POO$_{3/2}$]^0, 110Na$^+$, 25SO$_4^{2-}$	1.65 × 10^{22}	1.428 × 10^{22}

conductivity in the glass system. Here, we simulated the transfer mechanism of Na$^+$ to the neighbouring oxygen atom coordinated to the phosphate, as depicted in Scheme 1. The energies of intermediates and transition states were determined and are presented in Table 1. The calculated activation energies are consistent with the experimental values [28–30].

Dielectric response of these glasses has been examined by measuring both real and imaginary parts of the dielectric constants and electrical moduli. The real part of permittivity (ε') represents polarizability while the imaginary part (ε'') represents the energy loss due to polarization. Saltas et al. [52] and Kohr et al. [53] reported that dielectric materials have polarization mechanisms, viz. electronic, atomic orientation and interfacial effects. Figure 5 represents the variation of ε' with log(f) for NPM1 glass at different temperatures. Since the glasses investigated are ion conducting, low-frequency dispersion is quite high, which is generally attributed to electrode polarization [54] and is associated with the decrease in bond energies [55]. Dipolar polarization occurs with increase in temperature, which (i) weakens the inter-molecular forces, (ii) enhances the orientational vibrations and (iii) increases the thermal agitations. The polarizability contribution from ionic and orientation sources decrease at higher frequencies and disappear due to inertia of the ions.

The dielectric moduli (M$''$) as a function of frequency at different temperatures are shown in Fig. 6. The dielectric constants and dielectric moduli of the investigated glasses are qualitatively similar for all the investigated glasses. It is evident from Fig. 6 that M$''$ exhibits characteristically asymmetric peaks, which originate from the nature of the relaxation behaviour. As can be seen from Fig. 6, the frequency corresponding to relaxation peak is 'f$_0$' and the peaks shifted towards higher frequencies as the temperature was increased, which is in agreement with a thermally activated behaviour. The shape of the electrical relaxation does not depend on the temperature and composition. The variation of M$''$ with frequency is well fitted using Kohlrausch–Williams–Watts (KWW) or stretched exponential function for relaxation. The values of stretched exponent (β) were calculated assuming that M$''$ variation in frequency domain is due to a stretched exponential nature of relaxation $\varphi(t) = \varphi(0) \exp - \left(\frac{t}{\tau}\right)^{\beta}$ in time domain, using the empirical relation between β and full width at half maximum (FWHM) values of M$''$ peaks [54, 55]. The stretched exponent (β) extracted for all the glass and the values appear to be unaffected by the temperature. Temperature dependence of the imaginary part of the complex electrical modulus $M^*(\omega)$, measured as a function of frequency for NPM5 glass is shown in Fig. 6. The plots show features typical of relaxation. The temperature

Fig. 5 Variation of ε' versus log (f) for NPM3 glass
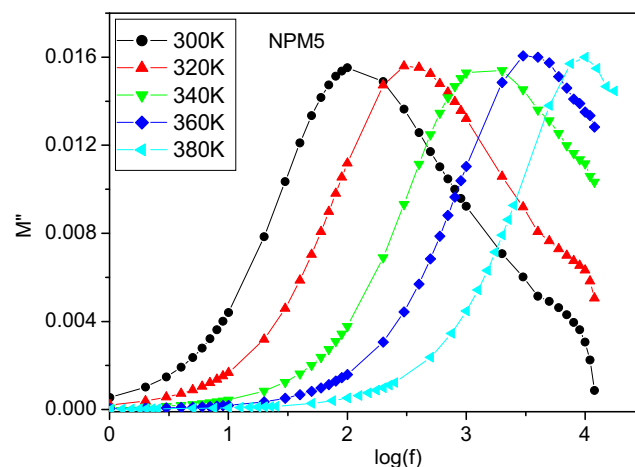
Fig. 6 Variation of M'' versus log (f)

dependence of the M'' peak, at which a resonance phenomenon occurs between the applied frequency and fluctuation of complex modulus $M^*(\omega)$, increases with increasing frequency. The relation between the modulus and the relaxation function is given by [56, 57]

$$M^*(\omega) = M_s\left[1 - \int_0^\infty \exp(i\omega t)\left(-\frac{d\varphi(t)}{dt}\right)dt\right]$$

where $M_s(=1/\varepsilon_\infty)$ is the electrical modulus value for $t = \infty$, where $\varphi(t)$ is a constant, is equal to zero, and hence is itself a constant. The calculation of modulus involves Laplace transform of the negative time derivative of the relaxation function $\varphi(t)$. Laplace transform does not exist for negative derivative of the KWW function mentioned above, except for β values of 1.0 to 0.5 [58]. Therefore, relation for $\varphi(t)$ has to be solved only by approximate methods for other values of β. One of the widely used methods is to expand the function as a series of exponential terms [49]. The microscopic origin of the KWW expression has been discussed by Ngai [59] in his coupling model, in which inter-ionic interactions cause a stretching of the relaxation time τ_c, which is defined as the most probable conductivity relaxation time and β is the stretched exponent. The smaller the value of β, the larger the deviation from Debye-type relaxation ($\beta = 1$). The β values extracted at 300 K are found to be 0.588, 0.589, 0.595, 0.610 and 0.612 when Na_2SO_4 varied from 5 to 25 mol%.

It is clear from Fig. 6 that M_{max} of the asymmetric peak shifts towards higher frequencies as the temperature is increased. The frequency corresponding to M_{max} will satisfy the condition $4\pi f_0\tau_c = 1$, where τ_c is the most probable conductivity relaxation time. Further, the electrical modulus behaviour of the present work is rationalized by invoking modified KWW function suggested by Bergman [60]. According to the modified KWW function, electrical modulus M'' can be written as
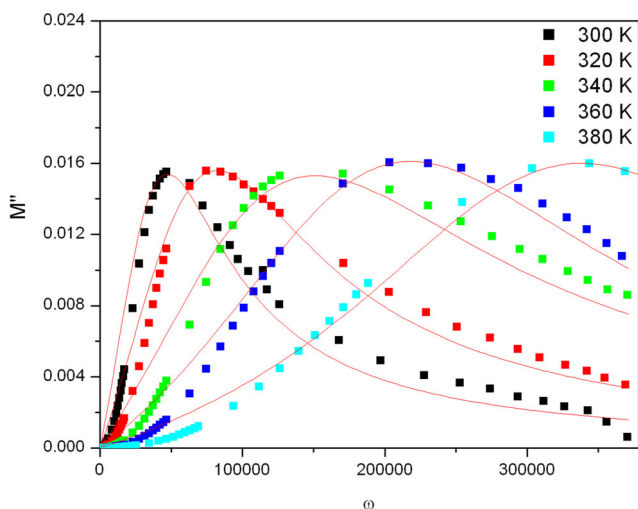

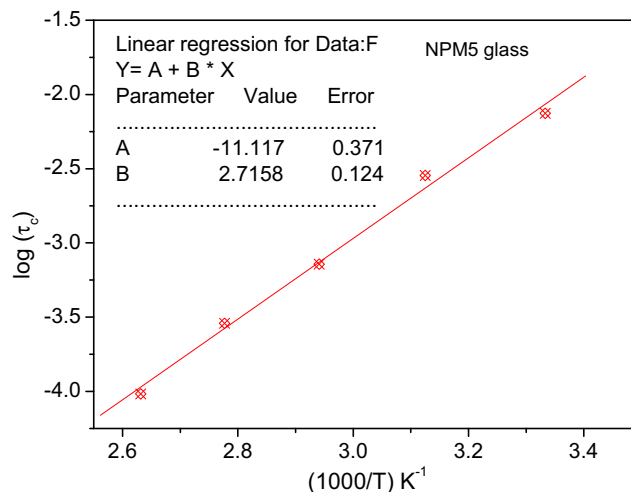**Fig. 8** Variation of $\log(\tau_c)$ versus $(1000/T)$. *Inset*: linear regression data

$M'' = \dfrac{M''_{max}}{(1-\beta)+\frac{\beta}{1+\beta}\left[\beta\left(\frac{\omega_{max}}{\omega}\right)+\left(\frac{\omega}{\omega_{max}}\right)^\beta\right]}$, where M''_{max} is the peak value of M'' and ω_{max} is the corresponding frequency. A theoretical fit of the above equation to the experimental data is shown in Fig. 7 as the solid line. It is seen from Fig. 7 that the experimental data is well fitted to this model except in the high-frequency regime and the β values are found to be temperature dependent [61, 62]. Figure 8 shows the reciprocal temperature dependence of the conductivity relaxation time, which obeys the Arrhenius relation, $\tau_c = \tau_0\, e^{\frac{E_{ac}}{kT}}$, where τ_0 is the pre-exponential factor ($\tau_0 = 3.07 \times 10^{-16}$s) and E_{ac} is the activation energy for conductivity relaxation. The activation (E_{ac}) energy is calculated by regression analysis and values are in the range 0.531 to 0.622 eV. These values compare well with the activation energy for the d.c. conductivity, which may be due to the fact that an ion has to overcome the same barrier while conducting as well as relaxing. In the process, M'' are scaled by M''_{max}, while the frequency axis is scaled by the relaxation
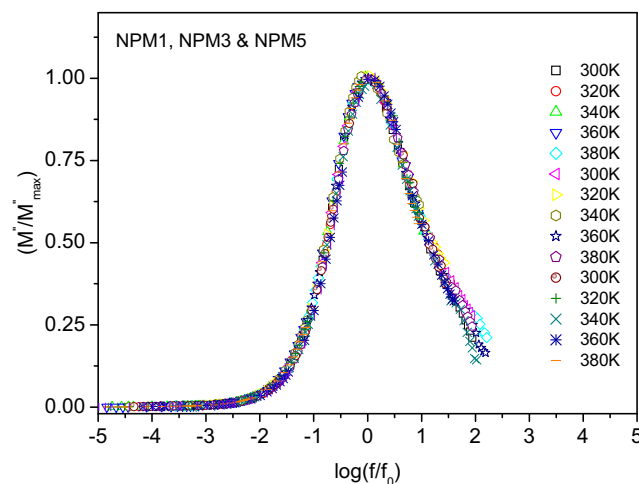

Fig. 7 Variation of M'' versus ω at different temperatures. *Solid lines* are theoretical fits

Fig. 9 Scaling of M''/M''_{max} versus $\log(f/f_0)$

frequency f_0. Hence, it is evident from Fig. 9 that the superposition of all data points of NPM1 and NPM3 glasses at different temperatures is satisfactory.

Conclusions

Molybdo-phosphate glasses containing Na^+ and SO_4^{2-} ions are prepared by an environment-friendly and energy-efficient microwave method. The amorphous nature was confirmed by X-ray diffraction and DSC studies. Thermal, electrical and dielectric properties of these glasses as a function of Na_2SO_4 content have been investigated. Isotropic dissolution of alkali salt in the glass network results in volume increasing effect. Consequently, density, Vickers hardness and T_g decrease with increasing concentration of Na_2SO_4. Impedance and electrical modulus investigations show the relaxation phenomenon with non-Debye type nature was confirmed. The activation energy, E_{dc}, for each glass was determined from the slopes extracted from log σ_{dc} versus $\frac{1000}{T}$ plots. The activation energies lie in the range 0.534 to 0.667 eV. These values are comparable with the conductivity measurements carried out using digital electrometer. The variation of dielectric constant as a function of frequency may be attributed to interfacial polarization. The dielectric data has been analysed using electrical modulus formalism and stretched exponential function φ $(t) = \varphi(0) \exp - \left(\frac{t}{\tau}\right)^\beta$, the conductivity relaxation time determined from modulus spectra was found to have activation energy (E_{ac}) close to those of E_{dc}, indicating migration of Na^+ ion through vacancies, which is responsible for both the ionic conduction as well as relaxation process. The activation energies calculated by ab initio method is comparable with the experimental values. Furthermore, the scaling of modulus data showed an excellent collapse on to a single master curve indicating that there is a good time–temperature superposition, and the conduction mechanism remains unchanged.

References

1. KJ Rao (2002) Structural chemistry of glasses, Elsevier
2. Angell CA (1990) Chem Rev 90:523–542
3. Elliott SR, Owen AP, Bunsenges BD (1991) Int J Phys Chem 95:987
4. Ngai KL (1996) J Non-Cryst Solids 103:232–245
5. Brow RK (2000) J Non-Cryst Solids 263:1–28
6. Narayana Reddy C, Veeranna Gowda VC, Sujatha B (2006) Ionics 12:159–165
7. Sujatha B, Narayana Reddy C, Chakradhar RPS (2010) Philos Mag B 90:632–2650
8. Chandra A, Bhatt A, Chandra A (2013) J Mater Sci Technol 29(3):193–208
9. Langar A, Sdiri N, Elhouichet H, Ferid M (2014) J Alloys Comp 590:380–387
10. Veeranna Gowda VC, Chethana BK, Narayana Reddy C (2013) Mater Sci Engg B 178:826–833
11. Sokolov IA, Murin IV, Kriyt VE, Pronkin AA (2011) Glass. Phys Chem 37(4):351–361
12. Nepomiluev AM, Pletnev RK, Lapina OV, Kozlova SV, Bamburov VG (2002) Glas Phys Chem 28:1–4
13. Careem MA, Mellander BE (1985) Solid State Ionics 15:327–330
14. Malugani JP, Meiez R, Fahys B, Robert G (1982) J Solid State Chem 45:309–316
15. Ganguli M, Harish Bhat M, Rao KJ (1999) Solid State Ionics 122:23–33
16. Nuchter M, Ondruschka B, Bonrathb W, Gum A (2004) Green Chem 6:128–141
17. Yasuoka M, Nishimura Y, Nagoka T, Watari K (2006) J Therm Anal Calorim 83:407–410
18. Vaidyanathan B, Agarwal DK, Roy R (2004) J Am Ceram Soc 87:834–839
19. Vaidhyanathan B, Rao KJ (1996) Bull Mater Sci 19:1163–1165
20. Klading WF, Horn JE (1990) Ceram Int 16:99–106
21. Komarneni S, Li Q, Stefansson KM, Roy R (1993) J Mater Res 8:3176–3183
22. Harish Bhat M, Chakravarthy BP, Ramakrishnan PA, Lavasseur A, Rao KJ (2000) Bull Mater Sci 23:461–466
23. Apte SK, Naik SD, Sonawane RS, Kale BB, Pavaskar N, Mandale AB, Das BK (2006) Mater Res Bull 41:647–654
24. Pitisescu RR, Barbara M, Marija K, Motoc A, Monty C, Iulia S, Kosmac T, Daskobler A (2004) J Euro Ceram Soc 24:1941–1944
25. Rao KJ, Mahesh K, Kumar S (2005) Bull Mater Sci 28:19–24
26. Vadivel Murugan A, Samuel V, Ravi V (2006) Mater Lett 60:479–480
27. Rao KJ, Vaidhyanathan B, Ganguli M, Ramakrishnan PA (1999) Chem Mater 11:882–895
28. MJ Frisch, GW Trucks, H B Schlegel et al (2009) Gaussian Inc, Wallingford CT
29. Wadt WR, Hay PJ (1985) J Chem Phys 82:284–298
30. Fischer G, Herler S, Mayer P, Schulz A, Villinger A, Weig JJ (2005) Inorg Chem 44:1740–1751
31. Selvaraj U, Sundar HGK, Rao KJ (1989) J Chem Soc, Faraday Trans 1 85(2):251–267
32. Bih L, Nadiri A, Aride J (2002) J Therm Anal Cal 68:965–972
33. Button DP, Tandon R, King C, Velez MH, Tuller HL, Uhlmann DR (1982) J Non-Cryst Solids 49:129–142
34. Ganguly R, Rao KJ (1999) J Non-Cryst Solids 2439:251–267
35. Cohen MH, Turnbull D (1959) J Chem Phys 31:1164–1169
36. Moynihan CT (1993) J Am Chem Soc 76(5):1081–1087
37. Barsoukov E, Macdonald JR (2005) Impedance spectroscopy: theory Experiment and applications. Wiley, USA
38. Dhaka R, Dhak D, Dosa M, Pramanik K, Pramanik P (2009) Mat Sci Eng B 164:165
39. Dyre JC (1988) J Appl Phys 64:2456–2468
40. Funke K, Banhatti RD (2006) Solid State Ionics 177:1551–1557
41. Vogel M (2004) Phys Rev B 70:94302–94310
42. Ingram MD, Jean Robertson AH (1997) Solid State Ionics 94:49–54
43. Dyre JC, Schroder TB (2000) Rev Mod Phys 72:873–892
44. Ravaine D, Soquet JL (1977) Phys Chem Glasses 18:27
45. Martin SW (1991) J Am Ceram Soc 74:1767–1784
46. Balakanski M, Wallis RF, Darianian I, Deepe J (1989) Mater Sci Eng B 3:15–21
47. Selvaraj U, Rao KJ (1985) J Non-Cryst Solids 72:315–334
48. Martin SW (1991) Eur J Sol State Inor 28:163–205

49. Souquet JL, Kone A, Ribes M (1980) J Non-Cryst Solids 3839: 307–310
50. Satyanarayana N, Karthikeyan A, Venkateswarulu M, Rambabu B (2001) Phys Chem Glasses 42:67–73
51. Bih L, El Omari M, Reau JM, Haddad M, Boudlich D, Yacoubi A, Nadiri A (2000) Solid State Ionics 132:71–85
52. Saltas V, Vallianatos F, Soupios P, Makris JP, Triantis D (2007) J Hazard Mater 142:520–525
53. Kohr SF, Talib ZA, Sidek HAA, Daud WW, Ng BH (2009) Am. J Appl Sci 6(5):1010–1014
54. Moynihan CT, Boesch LP, Laberge NL (1973) Phys Chem Glasses 14:122–125
55. Bhagat AA, Abou-Zeid YM (2001) Phys Chem Glasses 42: 361–370
56. Macedo PB, Moynihan CT, Bose R (1972) Phys Chem Glasses 13: 171–179
57. Kumar S, Rao KJ (2004) Chem Phys Lett 387:91–94
58. Elliott SR, Henn FEG (1990) J Non-Cryst Solids 166:179–190
59. Ngai KL, Rajgopal AK, Huang CY (1984) J Appl Phys 55: 1714–1716
60. Bergman R (2000) J App Phys 88:1356–1365
61. Majhi K, Vaish R, Parmesh G, Varma KBR (2013) Ionics (19): 99–104
62. Kundu S, Varma KBR (2014) J Am Ceram Soc 97(11):3582–3588